

Supporting information for:

**Redox Potential Tuning Through Differential
Quinone Binding in the Photosynthetic Reaction
Center of Rhodobacter sphaeroides**

Josh V. Vermaas,^{‡,§,||} Alexander T. Taguchi,^{‡,⊥,§,¶} Sergei A. Dikanov,[⊥] Colin A.
Wraight,^{‡,§} and Emad Tajkhorshid^{*,‡,§,||}

*Center for Biophysics and Computational Biology, Department of Biochemistry, Beckman
Institute, and Department of Veterinary Clinical Medicine, University of Illinois at
Urbana-Champaign, Urbana, Illinois 61801, United States*

E-mail: emad@life.illinois.edu

^aDeceased July 10, 2014

Running header

Quinone Differential Binding Modes in the Reaction Center

*To whom correspondence should be addressed

[‡]Center for Biophysics and Computational Biology

[§]Department of Biochemistry

^{||}Beckman Institute

[⊥]Department of Veterinary Clinical Medicine, University of Illinois at Urbana-Champaign, Urbana, Illinois 61801, United States

[¶]Current address: Department of Biochemistry and Molecular Biology, Nippon Medical School, Sendagi, Bunkyo-ku, Tokyo 113-8602, Japan

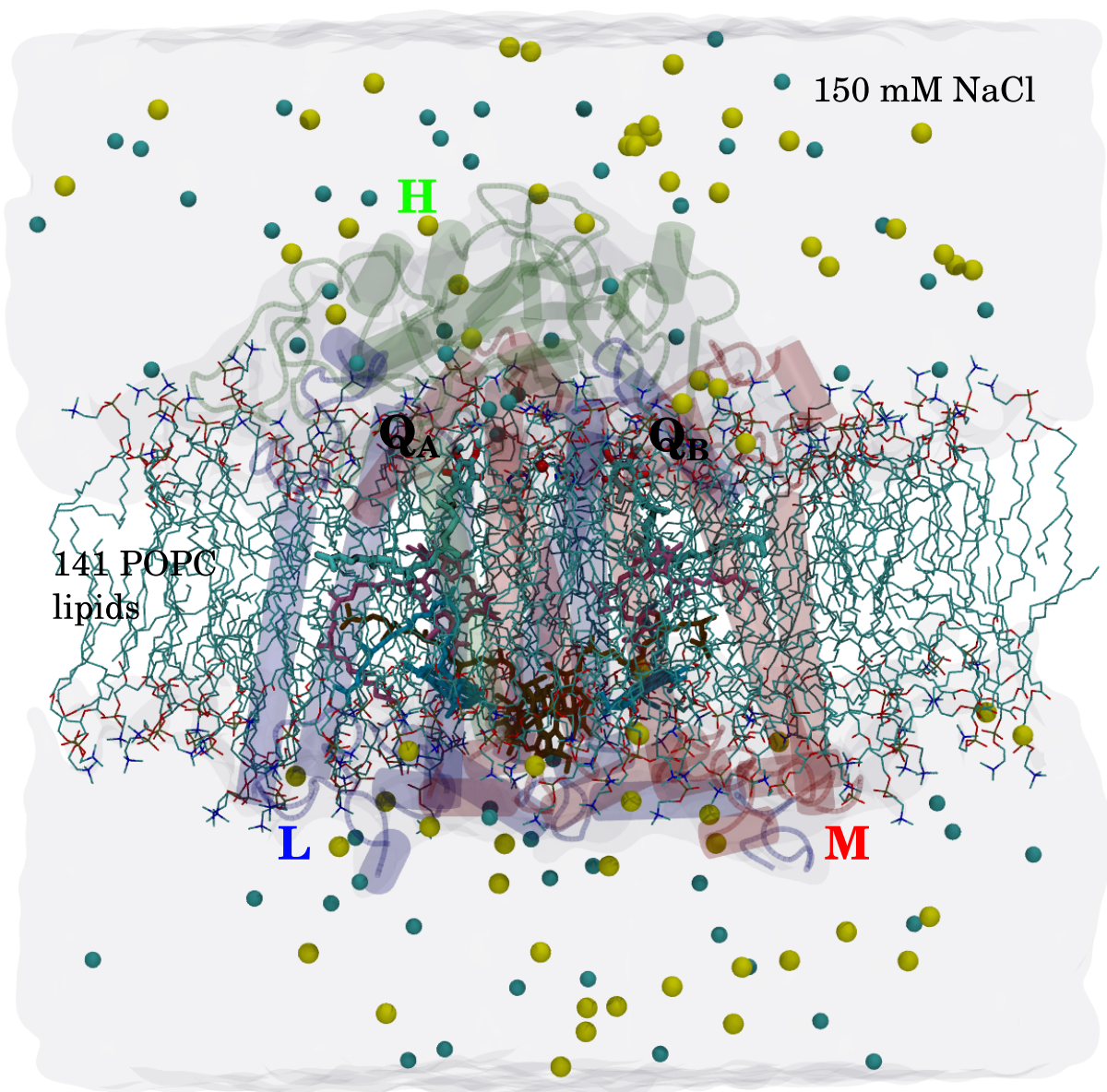


Figure S1: Complete simulation system of membrane-embedded RC. The RC itself is colored based on subunit (H is green, L is blue, and M is red). Within the RC, the cofactors are drawn in atomic detail, with the quinones outlined and colored more brightly than the other cofactors, as in Fig. 1. Beyond the protein, the embedding lipid bilayer is represented by lines (cyan is carbon, blue is nitrogen, red is oxygen, bronze is phosphorus). The surrounding solution is represented by the blue semi-transparent surface, and the ions are the spheres within the surface (yellow for Na^+ and cyan for Cl^-).

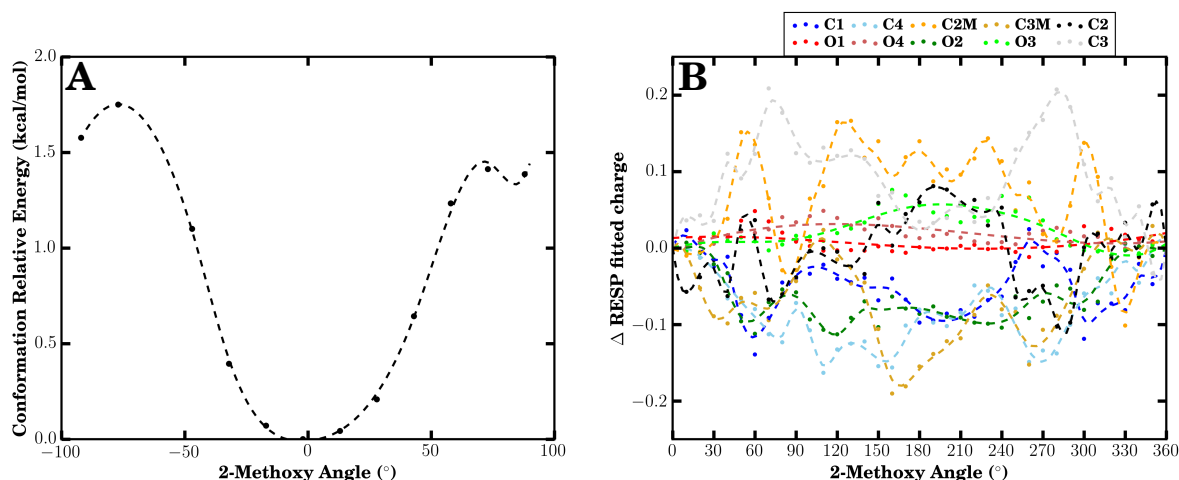


Figure S2: Effect of 2-methoxy rotation on quantum mechanical energy (A), and the derived RESP (Restrained Electrostatic Potential) charge distribution (B) in UbiQ. The energy minimum occurs when the methoxy group is in plane, however depending on its orientation, the charge distribution around the ring can change substantially, with the atoms showing the largest deviations highlighted. The carbonyl dipoles (C1, C4, O1, and O4) respond strongly, as do the methoxy oxygens and carbons (O2, O3, C2M, C3M, C2, and C3). The response is a result of electronic rearrangement around the π -system as a result of nuclear motion. In both panels, computed points are given as dots, with a smoothed spline fit also drawn to guide the eye.

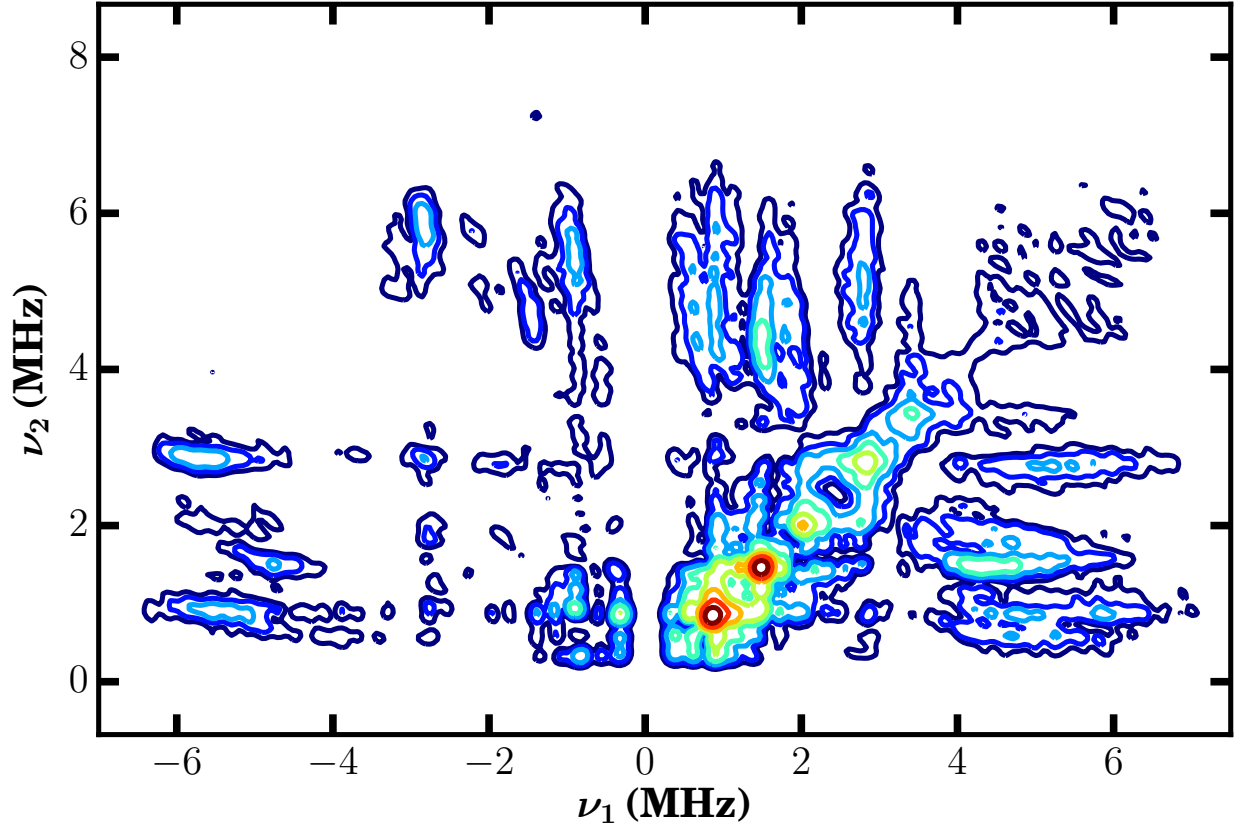


Figure S3: HSCORE measurements of the pH 10.5 borohydride reduced 3MeO-Q sample. The spectra shows features associated with Q_A^- , but not those associated with Q_B^- , suggesting that no Q_B^- is present in the sample. This implies that 3MeO-Q is unstable in the Q_B site, as detailed in the main text. HSCORE experimental settings: pulse sequence = $\pi/2-\tau-\pi/2-t1-\pi-t2-\pi/2-\tau$ -echo, $\tau = 136$ ns, microwave frequency = 9.634 GHz, magnetic field = 343.5 mT, temperature = 90 K. Time domain patterns were collected containing 256 x 256 points taken in 20 ns steps. Spectral processing of ESEEM patterns, including subtraction of the relaxation decay (fitting by 3rd degree polynomials), apodization (Hamming), zero filling, and fast Fourier transformation (FT), was performed using the Bruker WIN-EPR software.

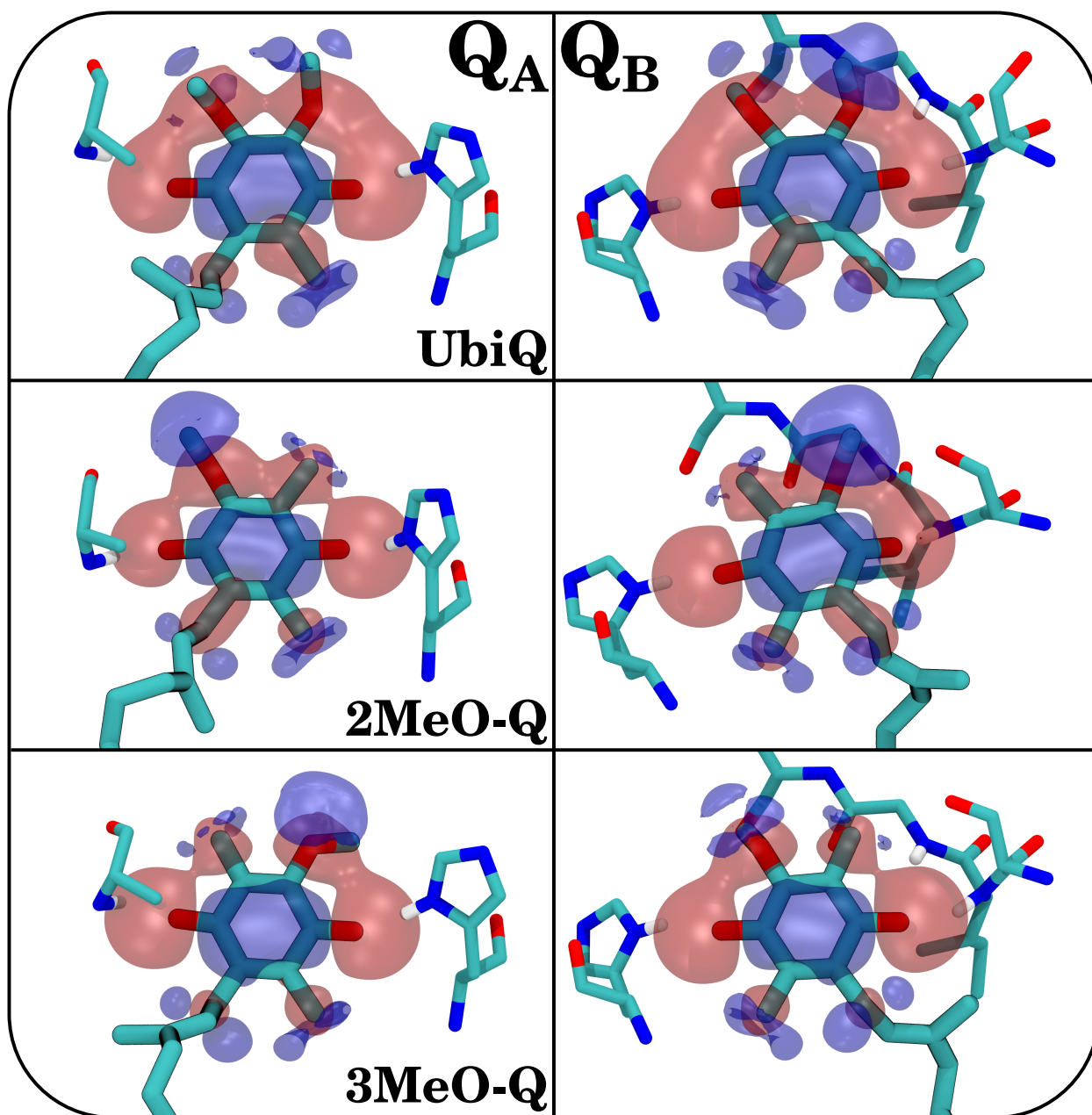


Figure S4: The electrostatic environment created by the different quinones in the Q_A and Q_B sites, along with their interaction partners for context. The shaded blobs represent positive (blue) and negative (red) potential energy surfaces averaged over the entire trajectory, drawn at the 40 kT/e level. At this detail, clear differences emerge between methoxy groups, particularly as it relates to where positive potential surfaces are located that would prevent the acceptance of hydrogen bonds, such as in 3MeO-Q Q_B .

Table S1: Counted transitions and residence time for the methoxy dihedral angles of UbiQ in propanol over 28.7 ns. The dihedral angles in solution transition rapidly between two states, one where the angle is positive, the other where the dihedral angle is negative, with a mean lifetime of only 0.7 ns for each state. Note that a transition was only counted when it reached an angle in excess of $\pm 40^\circ$, to avoid counting fluctuations about 0. The transition counts in parenthesis are scaled as if the source simulation was 300 ns, to allow for equitable comparison to Table S2.

	2-methoxy dihedral			3-methoxy dihedral		
	Transitions (Scaled)	$\tau_{>0}$ (ns)	$\tau_{<0}$ (ns)	Transitions (Scaled)	$\tau_{>0}$ (ns)	$\tau_{<0}$ (ns)
UbiQ	42 (439)	0.68	0.69	41 (429)	0.67	0.72

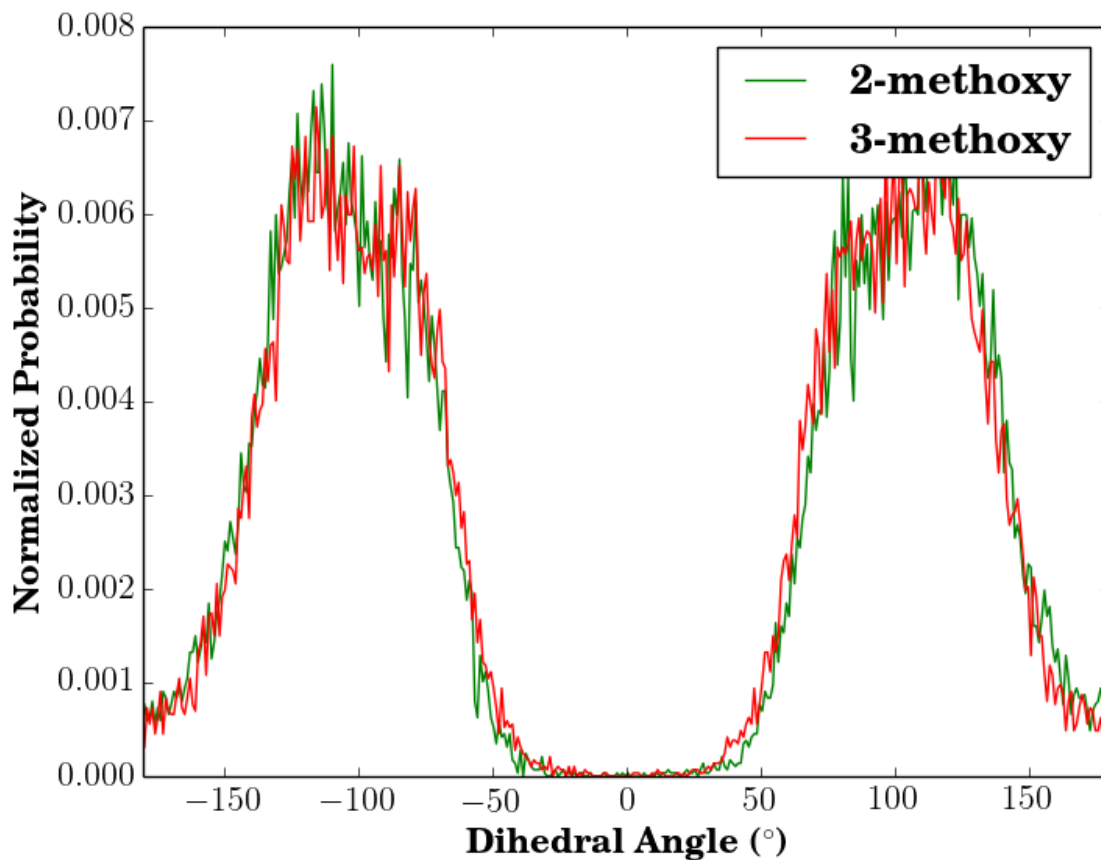


Figure S5: Dihedral angle distribution for UbiQ in propanol over a 28.7 ns equilibrium simulation. The mean position of the main peaks are at $\pm 107.2 \pm 0.2$ degrees for the 2-methoxy dihedral angle and $\pm 104.6 \pm 0.2$ degrees for the 3-methoxy dihedral angle.

Table S2: Counted transitions and residence time for the methoxy dihedral angles in the Q_A and Q_B sites over the 300 ns equilibrium simulations. With the exception of the 2-methoxy dihedral in Q_B , all dihedrals show frequent transitions over the course of the calculated trajectories. The mean residence time (τ) for dihedral values either greater than 0 ($\tau_{>0}$) or less than 0 ($\tau_{<0}$) are given where possible. As in Table S1, a transition was only counted when it reached an angle in excess of $\pm 40^\circ$, to avoid counting fluctuations about 0.

Quinone	2-methoxy dihedral			3-methoxy dihedral		
	Transitions	$\tau_{>0}$ (ns)	$\tau_{<0}$ (ns)	Transitions	$\tau_{>0}$ (ns)	$\tau_{<0}$ (ns)
Q_A Ubiquinone	213	0.9	1.9	46	1.4	11.6
MonomethoxyQ	240	2.0	0.5	74	0.5	7.5
Q_B Ubiquinone	2	0.3	299.7	50	1.8	10.2
MonomethoxyQ	0	–	–	129	3.2	1.5

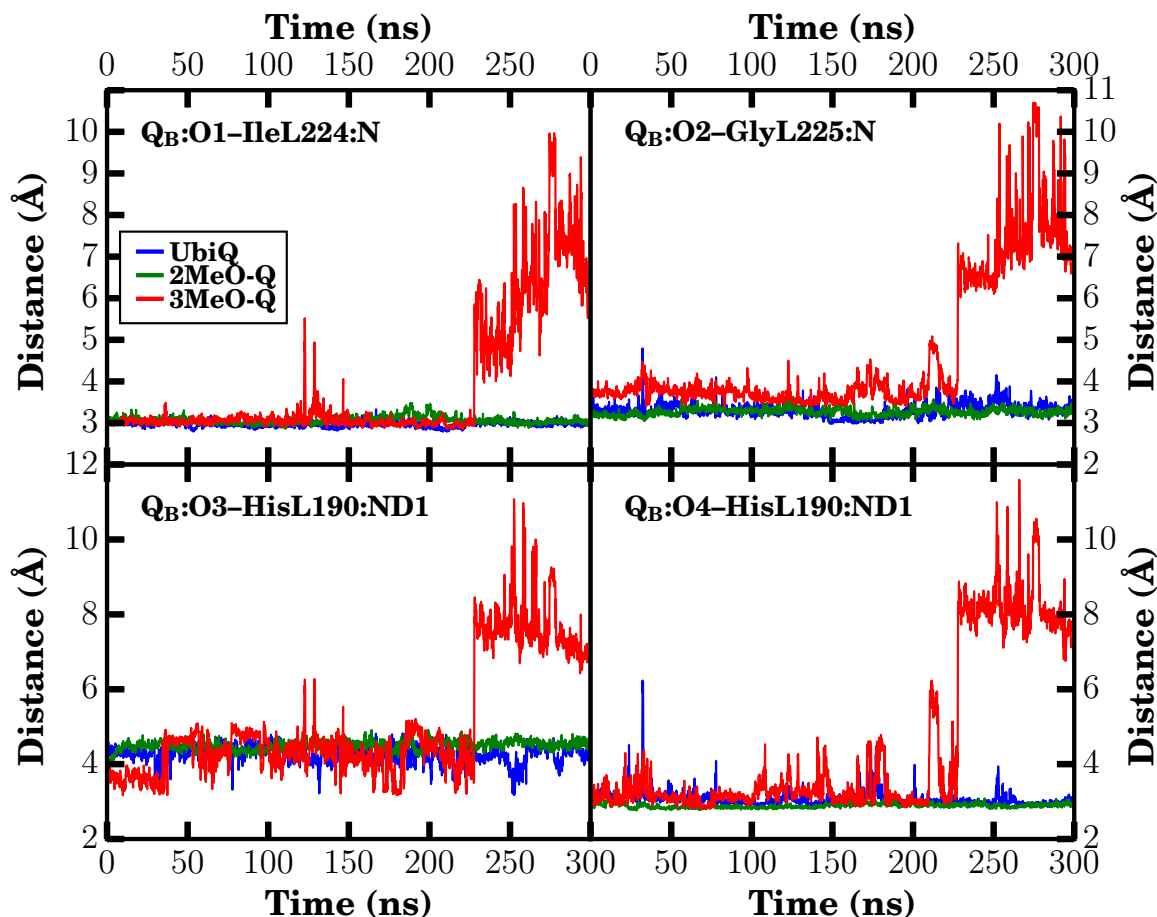


Figure S6: Full range interaction distances for carbonyl oxygen interactions in Q_B , showing the departure of 3MeO-Q to the distal site. The distance between the heavy atoms for each specific interaction was monitored over all three equilibrium trajectories (UbiQ is blue, 2MeO-Q is green, and 3MeO-Q is red). If the oxygen is missing for a particular interaction, the distance was determined based on the methyl carbon that replaced it. Note that 3MeO-Q moves to the distal site after 225 ns. Individual plotted datapoints are the running average over 100 ps of trajectory (the average of 50 frames with 2 ps intervals).

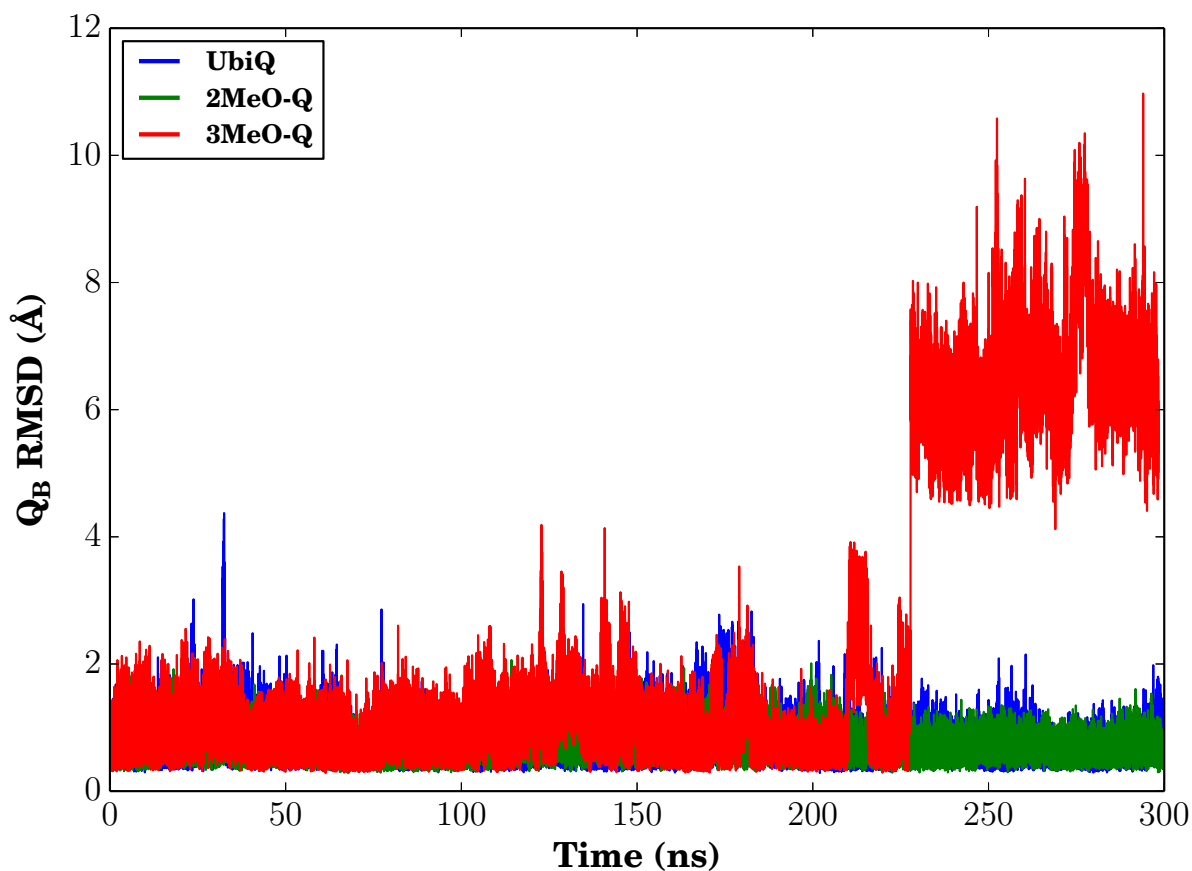


Figure S7: Mean RMSD of the quinone occupying the Q_B site relative to the proximal Q_B position observed in the 32 crystal structures with better than 2.8 \AA resolution. The RMSD was calculated by first aligning HisL190 and residues L223–L225, then measuring the RMSD of the 6 carbons comprising the benzene ring of the quinone between the simulation trajectory against all 32 crystal structures and reporting the mean thereof. Since there is not a perfect overlap between the 32 crystal structures, an RMSD of 0 is unattainable.

Table S3: Selected bond lengths from proximal Q_B quinones in the PDB. Distances are calculated to specific functional groups of a particular residue. For SerL223, the measurements are to the hydroxyl oxygen, for IleL224 and GlyL225, the measurements are to the backbone nitrogen, for AspL213, the measurement is to the carboxy oxygen nearest to SerL223, and to the $Q_B:O1$ or $Q_B:O2$ sites of UbiQ in the Q_B site as indicated.

PDBID-Chain	Distances (Å)					
	SerL223-AspL213	SerL223- $Q_B:O1$	IleL224- $Q_B:O1$	GlyL225- $Q_B:O1$	IleL224- $Q_B:O2$	GlyL225- $Q_B:O2$
1AIG-L	3.07	3.21	2.96	3.27	4.84	3.26
1AIG-N	2.78	3.05	2.76	3.20	4.75	3.34
1DV3-L	2.45	3.27	2.85	3.11	4.98	3.36
1DV3-R	2.43	3.12	2.63	2.89	4.93	3.31
1E14-L	2.51	2.58	2.81	3.04	4.96	3.26
1F6N-L	2.58	2.74	3.19	4.09	4.12	3.00
1QOV-L	2.58	2.66	2.96	3.24	4.92	3.27
1RG5-L	2.82	2.72	3.17	3.29	5.19	3.46
1RGN-L	2.93	2.51	3.18	2.91	5.43	3.68
1RQK-L	2.60	2.58	3.34	3.05	5.44	3.68
1RY5-L	4.71	2.67	2.82	3.14	4.94	3.29
1S00-L	2.72	2.73	2.80	2.77	5.27	3.53
1S00-R	2.82	2.71	2.51	3.08	4.75	3.28
2BOZ-L	2.43	2.78	2.74	3.13	4.84	3.19
2GNU-L	2.47	3.97	3.15	4.81	3.41	3.26
2HG3-L	2.75	2.67	2.98	3.32	4.94	3.28
2HG9-L	2.99	2.69	2.99	3.32	4.85	3.27
2HH1-L	2.97	2.75	2.89	3.24	4.78	3.22
2HHK-L	2.93	2.90	2.90	3.31	4.74	3.20
2HIT-L	2.82	2.68	3.11	3.50	4.85	3.38
2J8C-L	2.60	2.29	3.11	3.37	4.75	3.24
2J8D-L	2.59	2.60	3.36	2.68	5.74	3.88
2JIY-L	2.74	2.58	2.80	3.17	4.84	3.21
2JJ0-L	2.85	2.64	2.99	3.26	5.02	3.33
3DU3-L	–	3.04	2.83	3.54	4.47	3.13
3DUQ-L	–	3.04	2.83	3.59	4.49	3.03
3I4D-L	2.51	2.60	2.77	3.10	4.71	3.13
3ZUM-L	2.66	2.67	3.01	3.08	4.90	3.23
3ZUW-L	2.76	2.77	2.82	3.17	4.68	3.01
4IN5-L	2.58	2.48	2.82	2.85	5.05	3.28
4IN6-L	2.97	2.31	3.02	3.43	4.92	3.27
4RCR-L	3.66	2.74	3.25	3.28	5.50	3.85
Mean	2.81	2.77	2.95	3.26	4.87	3.32

Additional Computational Methods Description

Parameterization Details

For each model compound, several calculations were performed using Gaussian 09 to generate the quantum mechanical target data, using *ffTK* to setup Gaussian input files. The first step optimized the geometry of the model compound in vacuum at a MP2/6-31G* level of theory. *ffTK* used this optimized geometry as input to determine which atoms could act as hydrogen bond donors or acceptors, and for each potential interaction, positioned a water molecule appropriately. These water interactions, calculated at a HF/6-31G* level of theory as is done in the rest of the CHARMM force field, served as the quantum mechanical target data for the charge optimization protocol, assisted by *ffTK* to optimize the overall dipole of

the molecule as well as the optimal water interaction distances and energies in a molecular mechanics force field. The target data for the remaining terms was calculated at a MP2/6-31G* level of theory. Bond and angle terms originated from a Hessian calculation. Non-redundant torsions were detected by *ff*TK and scanned in order to parameterize dihedral terms. Optimization of the parameters against the quantum mechanical target data was carried out using the tools provided by *ff*TK, with manual tuning of the parameter set to assist the minimizers within *ff*TK away from unphysical solutions.

FEP Parameters

The FEP solvation free energy calculations were carried out in 50 equally spaced windows in λ (reaction coordinate) space, where $\lambda = 0$ represents a quinone fully decoupled from the solvent, and $\lambda = 1$ represents a fully coupled quinone. Each window was run for 1.2 ns, of which the last 1 ns was used to calculate the free energy change. A scaled-shifted soft-core potential was used for van der Waals interactions to minimize singularities for small values of λ . Electrostatic interactions were turned off when $\lambda < 0.3$ to avoid simulation instability due to the relative strength of electrostatic interactions compared with soft-core potential steric interactions.

Equilibration Protocol

Prior to production, 10 ns of equilibration was conducted for each equilibrium simulation. During the initial 10 ns equilibration, heavy atoms of the protein backbone were constrained in space with an exponentially decaying force constant, $k = 5e^{-t\text{ns}^{-1}}$ kcal/mol/Å², and carbons of the UbiQ ring were constrained with an exponentially decaying force constant of $k = 25e^{-t\text{ns}^{-1}}$ kcal/mol/Å². This equilibrated structure also served as the starting point for the FEP and TI calculations.

TI parameters

The reaction coordinate for the calculated transitions, distinct from the solvation free energy transition but also denoted by λ , ranged from 0 to 1, corresponding to the gradual replacement of UbiQ by the MMQ derivative with increasing λ . The transition was carried out by simulations at 17 intermediate λ values as well as the two end-points, specifically at $\lambda \in \{0, 0.02, 0.05, 0.1, 0.15, 0.2, 0.25, 0.3, 0.4, 0.5, 0.6, 0.7, 0.75, 0.8, 0.85, 0.9, 0.95, 0.98, 1\}$. The van der Waals contributions of UbiQ were reduced in concert with increasing the van der Waals contributions from the MMQ derivative with increasing λ . Electrostatic contributions from UbiQ were reduced to 0 as $\lambda \rightarrow 0.5$, and then added from the MMQ derivative when $\lambda > 0.5$. In this manner, the hybrid quinone is uncharged when $\lambda = 0.5$.

Why $\frac{1}{2}RT$?

Within the confines of the protein, the sampling of the methoxy dihedral angle is retarded. In solution, the mean lifetime for one state of the dihedral is 0.7 ns (Table S1), while the

predominant state of the dihedral might have a mean lifetime of 10s–100s of nanoseconds within the RC (Table S2). The net effect is that while the simulations used to calculate $\Delta G_{\text{UbiQ} \rightarrow \text{MMQ}}^{\text{m}}$ and $\Delta G_{\text{UbiQ} \rightarrow \text{MMQ}}^{\text{s}}$ adequately sample the additional rotational degree of freedom present in UbiQ, the simulations calculating the $\Delta G_{\text{UbiQ} \rightarrow \text{MMQ}}^{\text{p}}$ leg of the cycle in Fig. 3 do not sufficiently sample the rotation of the additional methoxy group. Given the long lifetime of the dihedral state in UbiQ (Table S2), explicitly sampling this degree of freedom is impractical, as it would require prohibitively long simulation per intermediate λ value. Thus we approximate the slow transition by correcting the final $\Delta\Delta G$.

Thermodynamic Integration without Restraints

Additional TI calculations were conducted without the use of restraints, which yielded counterintuitive results, primarily due to poor convergence at extrema in λ even with the use of soft-core potentials. Our initial approach was to use 20 ns of TI simulation after 0.5 ns equilibration using the same λ schema as was presented in Methods but without the restraining potential applied to the quinone rings. The final result (Tab. S4) in this case is significantly different from the final result presented in the main text, with some alarming conclusions. Without restraints, 3MeO-Q appears to bind more tightly to Q_{B} , a curious result in light of the missing interaction partner and in sharp contrast to the observed departure of 3MeO-Q from the proximal site during the equilibrium simulations. In addition, the results for 2MeO-Q suggest that it should bind less favorably than UbiQ to the Q_{B} site, despite its increased hydrophobicity and strong interaction with GlyL225.

The reason for this apparent inconsistency is the manner in which these quantities are calculated. TI, as the name implies, requires the computation of an integral, specifically:

$$\Delta G_{\lambda_0 \rightarrow 1} = \int_0^1 \frac{dG}{d\lambda} d\lambda = \int_0^1 \frac{dU}{d\lambda} d\lambda$$

From the TI calculations, we compute the value of $\frac{dU}{d\lambda}$ at different values for λ , fit these values to a smooth function, and integrate. Typically, the unrestrained TI calculations suffer from catastrophic divergence for the van der Waals terms when the quinone interacts weakly with its surroundings (Fig. S8). Since each quinone head was separately parameterized, the entire quinone headgroup is undergoing the alchemical transition independently, as the two are only coupled via the shared isoprene tail. As a result, when the quinone interacts only weakly with its surroundings, it is gas-like, and will come in close proximity to atoms in its surrounding, resulting in large values for $\frac{dU}{d\lambda}$. These artificially large $\frac{dU}{d\lambda}$ dominate the integral, and small errors in interpolation near the edges can yield vastly different results. Applying restraints to the heavy atoms of the quinones solves the problem by tethering the gas-like quinone to the quinone that is nearly fully present, which prevents the gas-like quinone from sampling unphysically close to surrounding atoms and accelerates convergence. These constraints do not impact the interactions, as demonstrated by the nearly identical integral values and lineshapes of the electrostatic component of $\frac{dU}{d\lambda}$ (Fig. S8)

Table S4: Relative binding affinities determined by TI calculations for UbiQ transformation into a MMQ without applied restraints. Relative binding free energies ($\Delta\Delta G$) are calculated as follows: $\Delta G_{\text{MMQ}}^{\text{s}\rightarrow\text{p}} - \Delta G_{\text{UbiQ}}^{\text{s}\rightarrow\text{p}} = \Delta G_{\text{UbiQ}\rightarrow\text{MMQ}}^{\text{p}} - \Delta G_{\text{UbiQ}\rightarrow\text{MMQ}}^{\text{s}} = \Delta\Delta G_{\text{UbiQ}\rightarrow\text{MMQ}}^{\text{s}\rightarrow\text{p}}$.

Site	MMQ	$\Delta\Delta G_{\text{UbiQ}\rightarrow\text{MMQ}}^{\text{s}\rightarrow\text{p}}$ (kcal/mol)
Q _A	2MeO-Q	-0.92 ± 0.02
	3MeO-Q	-0.62 ± 0.02
Q _B	2MeO-Q	0.22 ± 0.02
	3MeO-Q	-0.36 ± 0.01

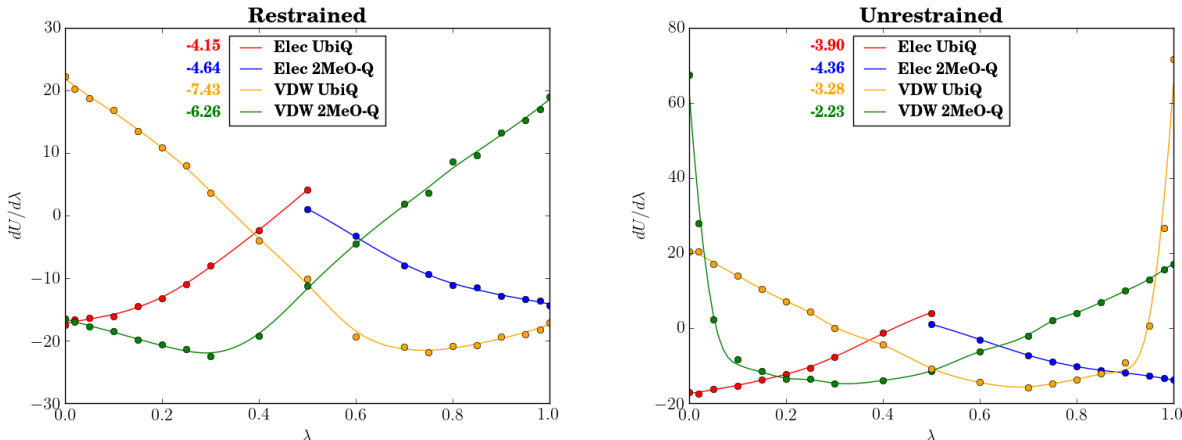


Figure S8: Representative comparison (specifically for the alchemical transformation for 2MeO-Q in solution) between restrained (left) and unrestrained (right) values for $dU/d\lambda$ as a function of λ . Integrals are broken down into their electrostatic and van der Waals (VDW) components, with the value for the integral shown beside the legend in each plot. In the unrestrained case, there are large contributions to the VDW integrals when the species interacts only slightly with its surroundings. This converges only very slowly, and the answer can change greatly depending on how the integral is calculated. With restraints, clashes with the environment at the integral endpoints are avoided, allowing for accurate computation of the underlying integrals.

Table S5: SerL223 interaction summary. The tabulated figures represent the percentage of the time where a particular hydrogen bond was formed to the hydroxyl group of SerL223. A hydrogen bond was defined to exist when the donor and acceptor heavy atoms are within 3.2 Å, and the hydrogen is within 30° of the line connecting them.

SerL223:OH Interaction Partner	Deprotonated AspL213	Protonated AspL213
AspL213	57.92	10.57
ArgL217	12.68	34.19
UbiQ	0.16	0.17